ACS APPLIED MATERIALS & INTERFACES

Research Article

www.acsami.org

Functionalized Graphene Nanoribbon Films as a Radiofrequency and Optically Transparent Material

Abdul-Rahman O. Raji,[†] Sydney Salters,[†,‡] Errol L. G. Samuel,[†] Yu Zhu,[†,§] Vladimir Volman,*[,∥] and James M. Tour*[,†,⊥,#]

[†]Department of Chemistry, [⊥]Department of Materials Science and NanoEngineering, [#]Richard E. Smalley Institute for Nanoscale Science and Technology, Rice University, 6100 Main Street, Houston, Texas 77005, United States

[‡]Second Baptist School, 6410 Woodway Drive, Houston, Texas 77057, United States

[§]Department of Polymer Science, The University of Akron, Akron, Ohio 44325, United States

[∥]Lockheed Martin, MS2, Mail Stop 137-101, 199 Borton Landing Road, Moorestown, New Jersey 08057, United States

Supporting Information

ABSTRACT: We report that conductive films made from hexadecylated graphene nanoribbons (HD-GNRs) can have high transparency to radiofrequency (RF) waves even at very high incident power density. Nanoscale-thick HD-GNR films with an area of several square centimeters were found to transmit up to 390 W (2×10^5 W/m^2) of RF power with negligible loss, at an RF transmittance of ~99%. The HD-GNR films conformed to electromagnetic skin depth theory, which effectively accounts for the RF transmission. The HD-GNR films also exhibited sufficient optical transparency for tinted glass applications, with efficient voltage-induced deicing of surfaces. The dispersion of the HD-GNRs afforded by their edge functionalization enables spray-, spin-, or blade-coating on almost any substrate, thus facilitating flexible, conformal, and large-scale film production. In addition to use in antennas and radomes where RF transparency is crucial, these capabilities bode well for the use of the HD-GNR films in automotive and general glass applications where both optical and RF transparencies are desired.

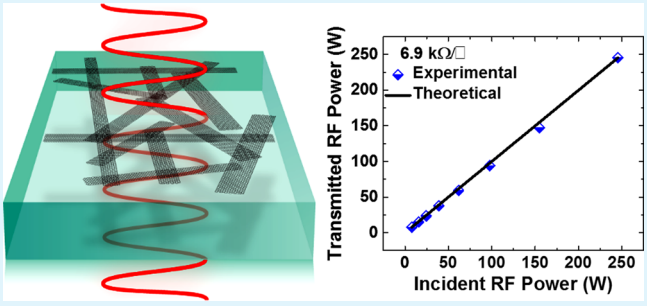

KEYWORDS: *functionalized graphene nanoribbon (GNR), Raman spectroscopy, radiofrequency (RF) transparent, RF transmittance, RF transmission loss, RF skin depth, carbon-based thin film, DC conductivity, RF conductivity, optical transparency, radome and antenna coating, resistive heating, deicing*

INTRODUCTION

Radiofrequency (RF) transmissions are used in a wide range of communication applications such as antennas and radomes, mobile services, and global positioning systems. We recently reported RF-transparent, electrically conductive hexadecylated graphene nanoribbon (HD-GNR) films for targeted voltage-induced deicing of RF equipment such as radar domes (radomes) and phased array antennas.[1] A large-scale HD-GNR composite film fabrication was demonstrated by spray-coating HD-GNRs on a polymer substrate whereby the HD-GNRs were embedded in polyurethane atop a polyimide flexible substrate rendering a black and optically opaque film. The HD-GNR films were transparent to RF, and they transmitted up to 20 W (7×10^3 W/m^2) of average RF power without significant loss. However, at >7×10^3 W/m^2 of average RF power density, there was some RF absorbance localized at thicker spots on the HD-GNR film that caused local increases in temperature. Subsequent thermal breakdown and carbonization of the polyurethane coating and polyimide substrate significantly reduced the RF transmittance. Thus, fabrication of highly uniform HD-GNR films would enhance RF transparency.

Though HD-GNRs films are not continuous films, they are composed of a percolating network of ribbons without any thick aggregates or random thick regions. Strong optical and RF absorption and scattering can occur on film surfaces where there are thicker regions and contaminants.[2−4] Although conductive carbon-based thin films have been heavily studied,[5−8] there is a lack of reports on conductive carbon-based films that are highly transparent to RF. Previous studies have reported on the electromagnetic shielding properties of carbon-based[9,10] and metal nanowire[11,12] films and composites in the RF/microwave region where the materials absorb a significant amount of the electromagnetic radiation. The HD-GNR films are an interlinked network, but the ribbons and pores are uniformly distributed and lack thick regions. This, combined with ultrathin film dimensions while also possessing

Received: June 2, 2014
Accepted: September 2, 2014
Published: September 4, 2014

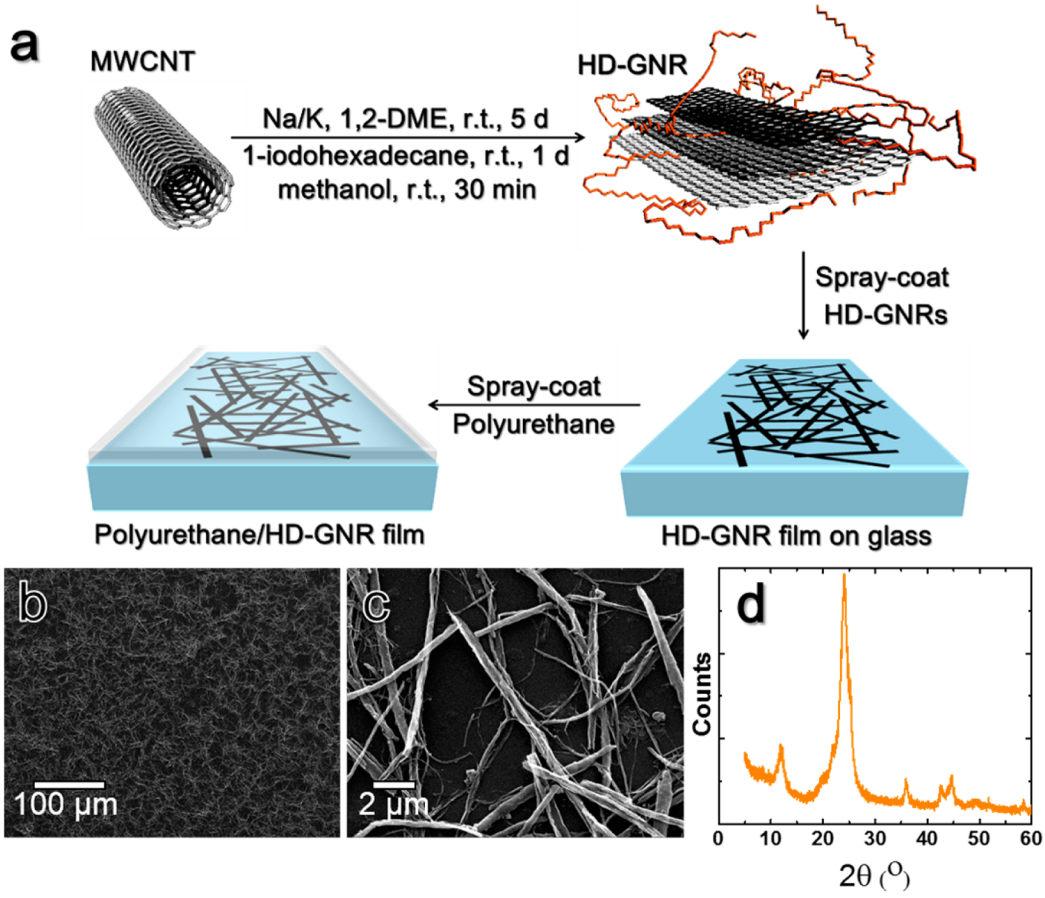

Figure 1. Fabrication and characterization of the HD-GNR film before coating with polyurethane. (a) Schematic of the HD-GNR synthesis and film fabrication. (b) SEM image of the HD-GNR film morphology. (c) SEM image of the HD-GNR film that shows HD-GNRs connected to form a percolating network. (d) X-ray diffractogram of the HD-GNR film. (e) Raman spectrum of the HD-GNR film.

significant optical transparency, supports excellent RF transparency that is consistent with theoretical values up to very high power density. Production of RF-transparent films that are also optically transparent while still being useful for deicing would extend applications to automotive glass and specialized window coating materials.[13,14]

Here, we report HD-GNR thin films that are highly RF-transparent, namely, up to a RF power density of $\sim 2 \times 10^5$ W/m^2 as permitted by the thermal capability of the underlying glass substrate. The HD-GNR films are also optically transparent enough for many tinted glass or plastics applications. Both the RF and optical transmittances vary with the sheet resistance of the HD-GNR films, which can be tuned on the basis of the film thickness. We expand a model based on skin depth theory to explain the RF transmission through the HD-GNR films. The skin depth (or decay length) of the RF wave in HD-GNR films is hundreds of microns, allowing RF transparency of subskin depth films. The quality and uniformity of the films is a contributing factor to the high RF transparency due to mitigation of thick HD-GNR regions or spots on the films. A voltage-induced deicing is also demonstrated.

EXPERIMENTAL METHODS

HD-GNR Synthesis and Film Preparation. *CAUTION: Na/K is a potent reductant and is highly reactive. All procedures involving Na/K alloy must be executed with extreme caution. The Na/K and the reaction mixture were prepared in a nitrogen-filled drybox and then sealed with a screw-cap and removed from the drybox, and the mixture was stirred with a magnetic stirrer in the hood. Piranha (used to clean the glass substrates) is a strong oxidant and must also be handled with care. Personal protective equipment including thick rubber gloves, a flame-retardant lab coat, goggles, and a face shield should be worn at all times during the experiment.*

Organic-soluble HD-GNRs were synthesized by splitting multiwalled carbon nanotubes (MWCNTs) using Na/K alloy in 1,2-dimethoxyethane and alkylating the edges with 1-iodohexadecane (Figure 1a).[15−17] Upon completion of the reaction, the Na/K alloy was *slowly and carefully* quenched with methanol and the product was washed sequentially with methanol, water, and diethyl ether. The sample was dried *in vacuo* for 24 h. (These HD-GNRs are now available commercially through AZ Electronic Materials Corp. and Sigma-Aldrich). The HD-GNRs were then suspended in *ortho*-dichlorobenzene (ODCB) at a concentration of 0.5 mg/mL and bath-sonicated for 15 min (12 W model 08849-00, Cole-Parmer) before use. The concentration of the HD-GNR solution was found to be optimal for spray-coating. Low concentrations required prolonged spraying to achieve the required film density. Concentrations that were too high made it difficult to finely control the film thickness to remain optically transparent. Nonfunctionalized GNR stacks were difficult to disperse in solvents[15] to form a stable dispersion for spray-coating films without thick spots. Functionalization with hexadecyl groups enabled dispersion in organic solvents, such as *ortho*-dichlorobenzene, as reported in our earlier work on HD-GNR synthesis where detailed solubility studies can be found.[15] Microscope soda lime glass slides (McMaster, 1 mm thick) were cleaned with piranha (7:4 v/v solution of H_2SO_4 and 35% H_2O_2), rinsed with copious amounts of deionized water, and blow-dried with a nitrogen stream. With an Iwata airbrush connected to compressed nitrogen, the HD-GNR solution was spray-

coated on the glass slide that had been placed on a hot plate heated to 200 °C. At this temperature, the HD-GNRs formed a uniform film on the glass with rapid evaporation of the solvent. After cooling to room temperature, polyurethane (clear-coat Dupli-Color auto paint, O'Reilly Auto Parts) was spray-coated over the HD-GNRs to provide a robust film. Since the HD-GNRs form a porous network on the glass, there is sufficient glass exposure for the adhesion of the polyurethane to the glass surface.

Characterization. SEM images were acquired on a JEOL 6500 SEM. Raman spectra of powdered samples placed on glass slides were acquired using a Renishaw inVia Raman microscope equipped with a 514 nm Ar ion laser. X-ray diffractograms were obtained on a Rigaku D/Max Ultima II Powder XRD with a Cu Kα (λ = 1.5418 Å) diffractometer using a zero background holder. Optical transmittance was obtained using a Shimadzu UV-3101PC UV−vis-NIR spectrophotometer. In order to determine the sheet resistance, the film resistance was measured using a two-terminal method with a Cen-Tech digital multimeter. This was further shown to be equivalent to four-terminal measurements (Figure S1, Supporting Information). To eliminate contact resistance between the probes and the film, silver electrodes were deposited by applying colloidal silver paste (Pelco Colloidal Silver Liquid, Ted Pella) on both ends of a 7.62 cm × 2.54 cm film; they were used for contact to the probes. Sheet resistance, R_S, was thus calculated on the basis of the measured resistance and film geometry with R_S = measured resistance × w/l where w and l are the width and length of the film, respectively. The DC conductivity, σ_0, was calculated with $\sigma_0 = (1/(R_S \times d))$ where d is the film thickness.

RESULTS AND DISCUSSION

The HD-GNR films consist of an isotropic array of HD-GNRs (Figure 1a). The films studied vary from 50 to 200 nm in thickness. Individual HD-GNRs are, on average, a 30 nm thick multilayer stack of HD-GNR layers.[15] They are 1 to 50 μm long (average ~10 μm) and 50 to 350 nm wide (average ~250 nm) (Figure 1b,c). On the basis of microscopic studies, the outer tubes are clearly split but whether the innermost tubes are split (Figure 1c) is uncertain. On the basis of the X-ray diffractogram in Figure 1d, the (002) peak of the HD-GNRs at 25.8° is close to that exhibited by a graphitic structure (26.3°) but with additional distinctive features. The pronounced asymmetry and shoulder of the (002) peak, coupled with the (001) peak at 12° is characteristic of intercalation with hexadecyl groups.[15] During the synthetic step at which the MWCNTs were treated with 1-iodohexadecane for edge functionalization, a significant amount of the moieties intercalated between the layers.[15]

Raman spectroscopy is a well-established technique for studying the stacking of graphene.[18−22] A multilayer graphene stack is not inevitably AB-stacked or graphitic.[19,23] Spectroscopic measurements are used here to determine the stacking order, or lack thereof, of the multilayer HD-GNRs. The strong characteristic Raman G and 2D bands at ~1587 and ~2688 cm^{-1}, respectively, indicate that the HD-GNRs maintain the basal plane π-conjugated sp^2-carbon structure.[15,16,19,24] Though the HD-GNRs are not monolayer, their Raman spectra exhibit features of monolayer graphene films. The Raman spectrum shows an I_G/I_{2D} ratio of 0.29 (Figure 2a), a single Lorentzian 2D band, and a 2D bandwidth of 40 cm^{-1} (Figure 2b). It is well-documented that monolayer graphene features an I_G/I_{2D} ratio of ≤0.50, a single Lorentzian 2D, a bandwidth of ≤33 cm^{-1}, and a 2D band position at 2680 cm^{-1}.[18−22,25,26] The $I_G/I_{2D} \leq 0.50$, upshifted 2D band position, and larger but single Lorentzian 2D bandwidth observed for the HD-GNRs compared to those for monolayer graphene have also been reported for nonoriented or non-AB-stacked multilayer graphene formed as-grown[23] or by folding[27,28] or *ex situ*

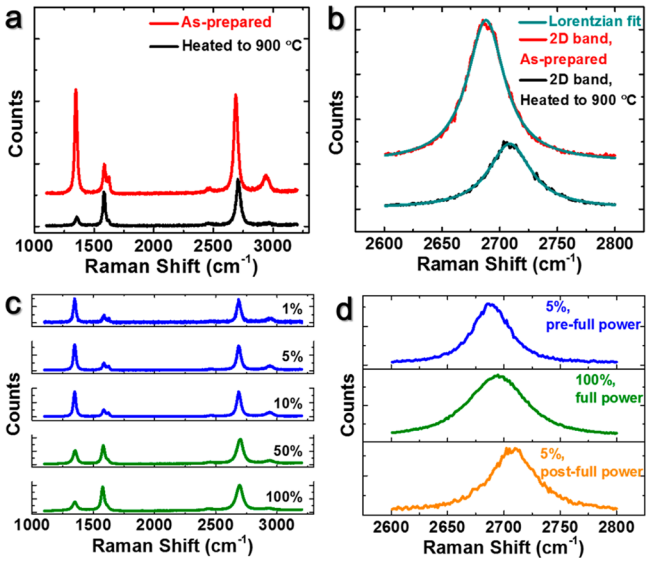

Figure 2. Raman spectroscopy of HD-GNRs. (a) Raman spectra of HD-GNRs, as-prepared (red) and heated to 900 °C (black). (b) 2D bands of HD-GNRs, as-prepared (red) and heated to 900 °C (black). Lorentzian fits of the 2D bands (cyan). (c) Excitation laser power effect on Raman spectrum of HD-GNRs. Spectra were collected from the same spot of the HD-GNR powder sample in the order presented in the plot. 100% power = 25 mW. (d) 2D bands of HD-GNR before and after measurement at 100% laser power.

stacking[18] of monolayer graphene films. The I_G/I_{2D} and line shape for monolayer graphene, non-AB-stacked graphene, and HD-GNRs are thus similar. These Raman features for multilayer graphene and HD-GNRs are due to nongraphitic stacking that exhibits weaker interlayer electronic interactions than the AB-stacked graphite.[19,26,29] In contrast, an AB-stacked graphite spectrum consists of a more intense G band and a strongly upshifted 2D band that has a larger bandwidth (>60 cm^{-1}) and that can be fitted with two Lorentzians.[19,26,30] As such, AB-stacked GNRs with 2 to 40 layers[24] were reported to feature Raman characteristics similar to those of graphite. The non-AB-stacked GNRs reported here can be called turbostratic graphene nanoribbons, multilayer graphene nanoribbons, graphene nanoribbon stacks, or simply, graphene nanoribbons.

The relative intensity of the D band with respect to the G band of HD-GNRs (I_D/I_G ratio ~3.7) is higher than that of defunctionalized HD-GNRs (I_D/I_G ratio ~0.23) (Figure 2a). The higher I_D/I_G ratio is attributed to the MWCNT splitting, hexadecylated edges, and intercalation of the HD-GNRs.[15] It should be noted that HD-GNRs, due to their relatively higher edge content, always show a larger D band[15,16] than their large graphene flake[18,25,31] or unfunctionalized GNR counterparts.[16,24] After heating the HD-GNRs to 900 °C under Ar at 20 °C/min, the I_D/I_G ratio is significantly reduced because of defunctionalization (Figure 2a).[15] Though edge-functionalized and intercalated edges are removed,[15] the non-AB stacking of the GNRs is retained as shown by Raman 2D band characteristics (Figure 2b).

During Raman measurements, a sufficiently low excitation laser power is critical in preserving the intrinsic Raman features.[26] Changes in the Raman spectral features of HD-GNRs could appear in the form of a change in I_D/I_G[32] or shifts of the Raman bands[32−35] due to laser-induced temperature effects. Laser powers of 2.5 mW or lower do not induce changes in the spectral features (Figure 2c). However, Raman

spectra obtained with a laser power of 12.5 mW or higher show smaller I_D/I_G ratios (Figure 2c) that arise from defunctionalization due to the laser-induced temperature increase. Thus, the Raman spectra obtained at a higher power alter the sample through defunctionalization, and the increase in temperature affects the analyses. Subsequent low power Raman analysis of the laser-heated sample shows that the 2D band is more upshifted than what is apparent during the relatively high power Raman measurement (Figure 2d). This result of low power measurement after laser-induced heating is consistent with the Raman spectrum of the thermally heated sample in Figure 2a.

Figure 3 shows the RF transmission measurements through HD-GNR films. For the highly uniform films produced in separate experiments on a glass substrate with sufficient thermal conductivity, the transmitted power increases linearly with the incident power. The RF transmittance was ~99% and ~98% for the two films of ~85 and ~110 nm thickness, respectively, and designated with red and blue dots, respectively, in Figure 2. Thus, there is a very small percentage of power loss during transmission up to 390 W (2×10^5 W/m^2) as permitted by the thermal capability of the substrate (Figure 3 inset). The linear relationship (slope = 1) between incident and transmitted RF indicates that the HD-GNR films are homogeneous, consistent with the SEM images. According to our previous work,[1] the transmitted power becomes nonlinear as the incident power increases for the reported nonhomogenous film. The transmitted power approached a plateau after 20 W (7×10^3 W/m^2) and subsequently dropped as the heating melted the polyurethane coating and further carbonized the polyurethane-coated polyimide substrate. This was attributed to the electromagnetic wave absorption and the resulting thermal energy concentration in the thick regions generated by nonuniform dispersion of the HD-GNR films where HD-GNRs were spray-coated at 200 °C atop polyurethane precoated on polyimide; the resulting coating was black and optically opaque. During the deposition, the nanoscale-thick polyurethane would be in a gel-like state and the underlying micron-scale-thick polyimide would buckle, yielding a nonuniform film with some thick regions. In the present work, however, the HD-GNR films were first deposited on a glass surface and polyurethane was deposited atop as a protection layer. Thus, the HD-GNR films formed a homogeneous percolating network on the glass without thick regions. Any GNR-thick regions would have been optically black, further resulting in significant RF absorbance since they are >250 nm thick. The fabrication of the uniform dispersion was done by monitoring the visual optical transparency and ensuring the absence of black, thicker locations. Optical transmittance measurements (discussed later) obtained at several locations on the film after fabrication were reproducible to ±2% (standard deviation), verifying the visual observation of uniformity. This uniformity proves to be essential for the desired RF transparency without the thicker regions that can significantly increase absorption at higher RF powers.

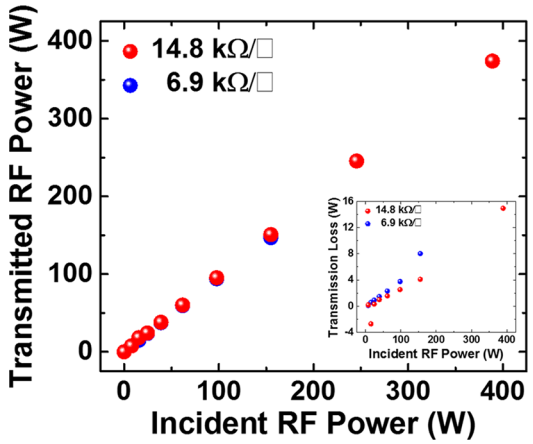

Figure 3. Transmitted vs incident RF power for two different films, designated with red and blue dots, sprayed to different thicknesses that had the designated sheet resistances of 14.8 kΩ/□ and 6.9 kΩ/□, respectively. Resistances were measured with a two point probe with silver electrodes at both ends of the film, and sheet resistance was calculated on the basis of the film geometry (Experimental Methods and Figure S1, Supporting Information). The transmitted powers are of the HD-GNR films only, and those of the protective polyurethane coatings were subtracted. Inset: Transmission loss vs incident RF power.

In describing waves propagation through the conductive HD-GNR film, the electric field component $\tilde{\mathbf{E}}$ (in V/m) of a uniform plane waves traveling in a given direction, z, perpendicular to the surface of the film, is given as eq 1:[36]

$$\tilde{\mathbf{E}}(z, t) = \tilde{\mathbf{E}}_0 e^{i(\tilde{k}z - \omega t)} \quad (1)$$

where $\tilde{\mathbf{E}}_0$ (in V/m) is the electric field vector parallel to the film surface and "$\tilde{k}$" (in 1/m) is the complex wavenumber such that eq 2 applies:

$$\tilde{k} = k + i\kappa \quad (2)$$

$\tilde{\mathbf{E}}$ is expressed in terms of the real and the imaginary parts of $\tilde{k}$ as in eq 3:

$$\tilde{\mathbf{E}}(z, t) = \tilde{\mathbf{E}}_0 e^{-\kappa z} e^{i(kz - \omega t)} \quad (3)$$

The imaginary part shows exponential attenuation of the amplitude $\tilde{\mathbf{E}}_0$ with respect to the distance z from the surface of the material. As a result, the distance through the material in which the field diminishes to 1/e or ~37% of its value from the surface satisfies eq 4:

$$\kappa z = 1 \quad \text{or} \quad z = 1/\kappa \quad (4)$$

This distance is referred to as the skin depth and will be denoted by Δ (in m) and eq 5 applies:

$$\Delta = \frac{1}{\kappa} = \frac{1}{\sqrt{\pi \sigma \mu_0 f}} \quad (5)$$

where σ is the material conductivity at frequency f and μ_0 is the permeability of free space, all in S.I. units. The skin depth characterizes the depth of electromagnetic wave propagation into a typical conductor. Since $e^2 \approx 10$, the electromagnetic wave loses 90% of its energy on its path at every skin depth. The application of this concept to describe RF transmission in HD-GNR thin films was previously suggested and proven through waveguide RF measurements at frequencies between 2 and 4 GHz.[1] It was demonstrated that, similar to classical conductors, the RF conductivity was very close to the DC conductivity of HD-GNR thin films.

When a traveling free-space plane-wave is incident on the front and back boundaries of an HD-GNR film, a portion of the wave energy is reflected from the film back to free space while the propagation continues inside the HD-GNR film.[36,37] As this propagated wave reaches the back boundary, it is reflected again in the direction of the front boundary with the phase shift $\varphi = kz$, and the remaining energy is transmitted to the free space

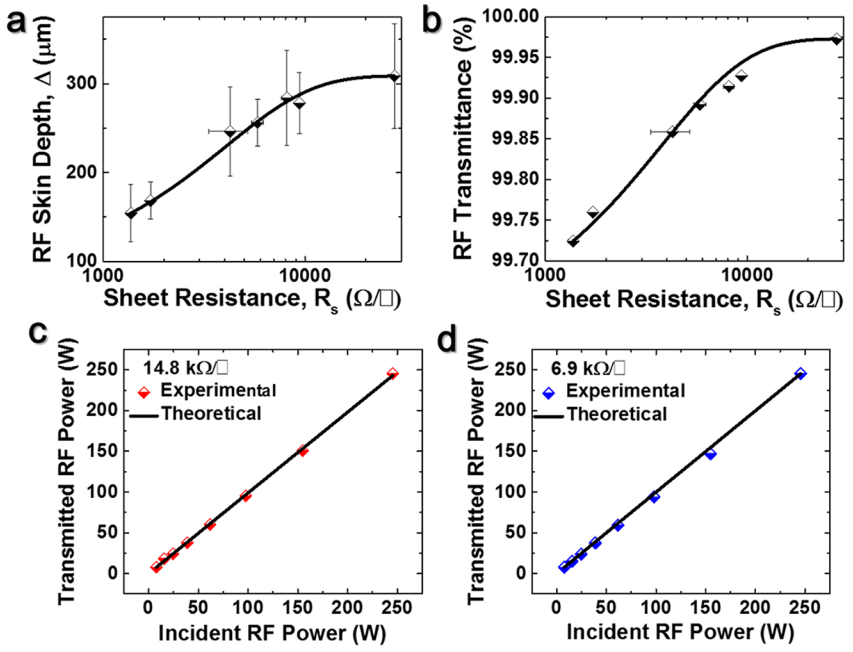

Figure 4. Predictions from electromagnetic skin depth theory. (a) Dependence of the theoretical RF skin depth on the sheet resistance of the HD-GNR film. (b) Dependence of the calculated RF transmittance on the sheet resistance of the HD-GNR. (c) Transmitted RF power (experimental and theoretical) vs incident RF power for a HD-GNR film with a resistance of 14.8 kΩ/□. (d) Transmitted RF power (experimental and theoretical) vs incident RF power for a HD-GNR film with a resistance of 6.9 kΩ/□.

behind the HD-GNR film. Therefore, the total reflected wave from the front boundary and transmitted wave through the film are superpositions of multiple partial waves moving back and forth. The total transmission loss is the sum of reflection/mismatch loss and HD-GNR absorption loss of the wave defined by eq 3, but the thickness of the HD-GNR film is such a small fraction of the wavelength that all the reflected waves at the front boundary are in almost opposite phases and cancel each other. In addition, since mismatch loss, from waveguide measurements, does not exceed 1% of incident power,[1] the main part of the loss is the HD-GNR absorption loss defined by the skin depth (eq 5) that increases at higher sheet resistance (Figure 4a) due to lower conductivity at higher sheet resistance (eq 5, Table S1, Supporting Information). Thus, the RF transmittance for a film is related to its skin depth Δ and thickness d by eq 6:[37]

$$T = P_T/P_0 = (E_{0,T}/E_{0,I})^2 = e^{-2d/\Delta} \quad (6)$$

where P_T and P_0 (in W) are transmitted and incident RF powers and $E_{0,T}$ and $E_{0,I}$ (in V/m) are transmitted and incident amplitudes, respectively, through the HD-GNR film. As with the skin depth, the RF transmittance increases with higher sheet resistance (Figure 4b). In order to validate this theory for HD-GNR films, the transmitted RF powers were compared with a series of incident RF powers for the two films measured in Figure 3. The results demonstrate an excellent match between the theoretical calculations and the experimental measurements (Figures 4c, d) for the sample HD-GNR films, thus supporting the classical conductivity behavior at radio frequencies. Thus, for a thin HD-GNR film, the wave propagates with an amplitude very close to that of the incident wave. As a result, the HD-GNR film is transparent to the RF wave.

Sheet resistances and optical transmittances of the HD-GNR films can also be tuned by varying the film thicknesses. In Figure 5a, the optical transmittance of the films increase with increasing sheet resistance. Images in Figure 5b show the decreasing optical transmittance of HD-GNR films from 75% to 50%. At > 65% optical transmittance, the sheet resistance of the HD-GNR film is ~6 kΩ/□. With this amount of resistance, the film is suitable as a thin film resistor where heating power $P = V^2/R$ can be delivered through the film subject to an applied voltage.

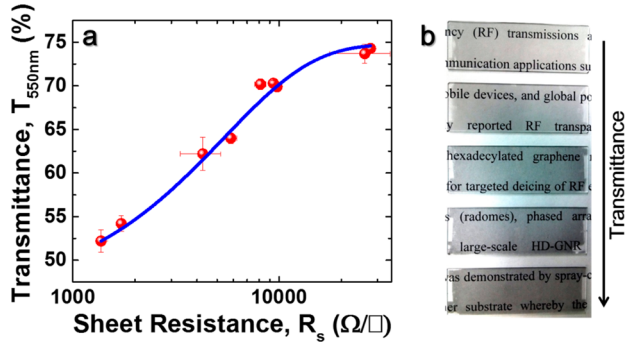

Figure 5. (a) Optical transmittance dependence on sheet resistance of HD-GNR films. The sheet resistances were measured as described in the Experimental Methods above using the two-terminal measurement technique (see Figure S1, Supporting Information, for comparison to four-terminal measurements). Transmittance of HD-GNR films at 550 nm vs sheet resistance. The resistances are of the HD-GNR films without polyurethane coating. (b) Photograph showing optical transparency through the HD-GNR films with transmittance from 75% (top) to 50% (bottom).

Though optical transparency is not essential in many applications of RF transparent conductive HD-GNR films, certain applications would require optical transparency in addition to RF transparency. The transmission properties of HD-GNR films in the visible region can be evaluated by

dx.doi.org/10.1021/am503478w | ACS Appl. Mater. Interfaces 2014, 6, 16661−16668

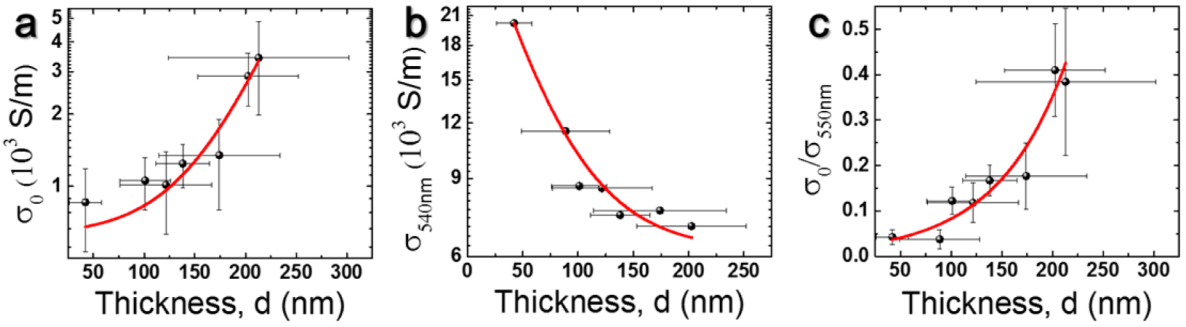

Figure 6. DC and optical conductivity of HD-GNR films. (a) DC conductivity of HD-GNR films as a function of thickness. (b) Optical conductivity of HD-GNR films as a function of thickness. (c) DC conductivity/optical conductivity ratio of HD-GNR films as a function of thickness. The conductivities and thicknesses are of the HD-GNR films without polyurethane coating.

studying the relationship between DC (i.e., zero frequency) and optical (i.e., frequency dependent) conductivities. The DC conductivity ($\sigma_0 = (1/(R_S \times d')$, Experimental Methods) of HD-GNR films is found to increase with the thickness (Figure 6a). The sheet resistance of a material depends on the thickness. However, the electrical conductivity of a uniform, homogeneous material is thickness independent provided that the uniformity is invariant with thickness. Thus, an increase in the DC conductivity is due to an increase in the film density rather than the film thickness. This behavior is similar to that observed for carbon nanotube[38,39] and silver nanowire films.[40] Unlike those films, however, the optical conductivity, σ_{550nm}, of HD-GNR films decreases with the film thickness (Figure 6b), producing an optical conductivity/DC conductivity ratio greater than unity ($(\sigma_{550nm}/\sigma_0) > 1$) (Figure 6c). This behavior is similar to that observed in chemically exfoliated graphene films.[41] Thus, the sheet resistance of the HD-GNR films is required to be high in order for the second term in eq 7, below, to approach zero so as to produce an optical transmittance that approaches unity or 100%:[38−40]

$$T = \left(1 + \frac{188\sigma_{550nm}}{R_S\sigma_0}\right)^{-2} \quad (7)$$

Film density is an important parameter for obtaining a low σ_{550nm}/σ_0; however, the thickness and width of individual components of the film have to be small as well in order to reduce the overall film thickness. Carbon nanotube films and silver nanowire films were reported to exhibit $(\sigma_{550nm}/\sigma_0) < 1$. The thickness of an individual carbon nanotube[39] was 2.4 nm, and an individual silver nanowire[40] was 85 nm. This enabled fabrication of sub-100 nm thick, dense films with high optical transmittance and low sheet resistance.[38−40] The foliated HD-GNRs (in stacks) reported here are ∼30 nm thick and ∼250 nm wide, and the films made from them are 50 to 200 nm thick. Since the optical conductivity/DC conductivity ratio of HD-GNR films decreases with higher film density thickness (Figure 6c), our results suggest that, if the individual HD-GNRs were of much smaller width and thickness, the film density could be significantly increased but with film thicknesses being much lower than those obtained here.[42] Thus, HD-GNR films with lower optical conductivity relative to the DC conductivity may be obtained, i.e., $(\sigma_{550nm}/\sigma_0) < 1$; a condition that would facilitate fabrication of HD-GNR films with high optical transmittance at low sheet resistance. However, efficient exfoliation of the GNRs derived from MWCNTs has been, hitherto, unattainable.[15−17]

In order to demonstrate deicing capability with the HD-GNR films, an HD-GNR film with a resistance of 3.8 kΩ was fabricated on a glass slide and mounted in a Styrofoam box cooled to −20 °C (Figure 7a). A voltage of 190 V was applied across the film through silver contacts on both ends providing ∼1.3 W/cm^2 to the film. The ice melted and then detached entirely in 3.7 min (Figure 7b), underscoring the deicing capability along with the RF and optical transparency discussed above.

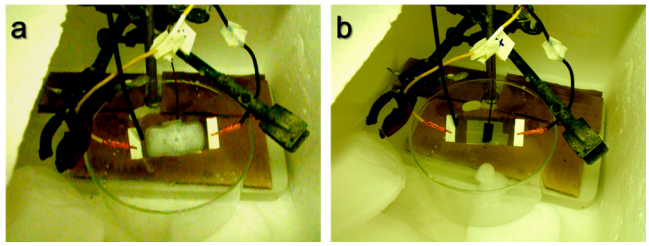

Figure 7. Photographs of resistively heated HD-GNR films at −20 °C. (a) During deicing. (b) After deicing which took 3.7 min. The experiment was conducted in a Styrofoam box maintained at −20 °C. The sample was mounted at an angle of ∼40° so that the partially melted ice could slide off. The ice that melted off the surface can be seen rapidly refreezing once it hits the dish below. A surface thermocouple was taped to the bottom of the polyurethane-HD-GNR-coated glass slide. All heating was done through an applied voltage to the left and right ends of the film. The HD-GNR film has a resistance of 3.3 kΩ, a thickness of 140 nm, and an optical transmittance (at 550 nm) of 70%.

CONCLUSION

In summary, we have demonstrated that conductive HD-GNR thin films can be produced with high uniformity. We verified 99% RF transmission at a power density up to 2×10^5 W/m^2 in an 85 nm thick HD-GNR film with an optical transmittance of 75%. The small HD-GNR film thickness relative to the large skin depth and propagation wavelength through the film permits the exceedingly high RF transmission at high RF power. The absence of thick spots and relatively high thermal conductivity of the substrate is crucial to transparency at high RF power. We also demonstrated the possibility of obtaining more optically transparent films with better exfoliated HD-GNRs. The optical transparency is important in controlling the quality of fabricated RF transparent films as optical transmittance could be easily measured at different regions of the film to assess uniformity and the presence of thick spots.

Finally, the RF and optically transparent films permitted voltage-induced deicing.

■ ASSOCIATED CONTENT

Supporting Information

Sheet resistances, conductivities and thicknesses; comparison between two and four terminal measurements of HD-GNR films. This material is available free of charge via the Internet at http://pubs.acs.org.

■ AUTHOR INFORMATION

Corresponding Authors

*E-mail: vlad.vlad@verizon.net.
*E-mail: tour@rice.edu.

Notes

The authors declare the following competing financial interest(s): Y.Z., V.V., and J.M.T. are co-inventors on patent applications (US201220808A1 and WO2012100178A1) owned by Rice University and Lockheed Martin Aerospace Co. which disclose the use of RF-transparent GNR films for radome deicing circuits.

■ ACKNOWLEDGMENTS

The Lockheed Martin Aerospace Co. through the LANCER IV Program supported the RF testing of the films, and the ONR MURI program (#00006766, N00014-09-1-1066) and the AFOSR (FA9550-09-1-0581) provided funding.

■ REFERENCES

(1) Volman, V.; Zhu, Y.; Raji, A.-R. O.; Genorio, B.; Lu, W.; Xiang, C.; Kittrell, C.; Tour, J. M. Radio-Frequency-Transparent, Electrically Conductive Graphene Nanoribbon Thin Films as Deicing Heating Layers. *ACS Appl. Mater. Interfaces* **2014**, *6*, 298−304.

(2) Zhang, P.; Lau, Y. Y.; Gilgenbach, R. M. Analysis of Radio-Frequency Absorption and Electric and Magnetic Field Enhancements due to Surface Roughness. *J. Appl. Phys.* **2009**, *105*, 114908.

(3) Bosman, H.; Lau, Y. Y.; Gilgenbach, R. M. Microwave Absorption on a Thin Film. *Appl. Phys. Lett.* **2003**, *82*, 1353−1355.

(4) Bosman, H.; Lau, Y. Y.; Gilgenbach, R. M. Power Absorption by Thin Films on Microwave Windows. *IEEE Trans. Plasma Sci.* **2004**, *32*, 1292−1297.

(5) Dan, B.; Irvin, G. C.; Pasquali, M. Continuous and Scalable Fabrication of Transparent Conducting Carbon Nanotube Films. *ACS Nano* **2009**, *3*, 835−843.

(6) Becerril, H. A.; Mao, J.; Liu, Z.; Stoltenberg, R. M.; Bao, Z.; Chen, Y. Evaluation of Solution-Processed Reduced Graphene Oxide Films as Transparent Conductors. *ACS Nano* **2008**, *2*, 463−470.

(7) Eda, G.; Lin, Y. Y.; Miller, S.; Chen, C. W.; Su, W. F.; Chhowalla, M. Transparent and Conducting Electrodes for Organic Electronics from Reduced Graphene Oxide. *Appl. Phys. Lett.* **2008**, *92*, 233305.

(8) Zhu, Y. W.; Cai, W. W.; Piner, R. D.; Velamakanni, A.; Ruoff, R. S. Transparent Self-Assembled Films of Reduced Graphene Oxide Platelets. *Appl. Phys. Lett.* **2009**, *95*, 103104.

(9) Li, Y.; Chen, Z.; Zhang, S.; Ni, Y.; Huang, J. Electrical Conductivity and Electromagnetic Interference Shielding Characteristics of Multiwalled Carbon Nanotube Filled Polyacrylate Composite Films. *Appl. Surf. Sci.* **2008**, *254*, 5766−5771.

(10) Song, W.-L.; Cao, M. S.; Lu, M.-M.; Bi, S.; Wang, C. Y.; Liu, J.; Yuan, J.; Fan, L.-Z. Flexible Graphene/Polymer Composite Films in Sandwich Structures for Effective Electromagnetic Interference Shielding. *Carbon* **2014**, *66*, 67−76.

(11) Hu, M.; Gao, J.; Dong, Y.; Li, K.; Shan, G.; Yang, S.; Li, R. K.-Y. Flexible Transparent PES/Silver Nanowires/PET Sandwich-Structured Film for High-Efficiency Electromagnetic Interference Shielding. *Langmuir* **2012**, *28*, 7101−7106.

(12) Yu, Y. H.; Ma, C.-C. M.; Teng, C.-C.; Huang, Y.-L.; Lee, S.-H.; Wang, I.; Wei, M.-H. Electrical, Morphological, and Electromagnetic Interference Shielding Properties of Silver Nanowires and Nanoparticles Conductive Composites. *Mater. Chem. Phys.* **2012**, *136*, 334−340.

(13) Stolhofer, D.; Doelecke, H.; Liu, Y.; O'eary, P. RF Propagation Through Transparent Conductors in Energy Efficient Windows. In *Proceedings of the 16th European Wireless Conference*, Lucca, Italy, April 12−15, 2010; IEEE: Piscataway, NJ, 2010.

(14) Granqvist, C. G. Transparent Conductors as Solar Energy Materials: A Panoramic Review. *Sol. Energy Mater. Sol. Cells* **2007**, *91*, 1529−1598.

(15) Genorio, B.; Lu, W.; Dimiev, A. M.; Zhu, Y.; Raji, A.-R. O.; Novosel, B.; Alemany, L. B.; Tour, J. M. *In Situ* Intercalation Replacement and Selective Functionalization of Graphene Nanoribbon Stacks. *ACS Nano* **2012**, *6*, 4231−4240.

(16) Kosynkin, D. V.; Lu, W.; Sinitskii, A.; Pera, G.; Sun, Z.; Tour, J. M. Highly Conductive Graphene Nanoribbons by Longitudinal Splitting of Carbon Nanotubes Using Potassium Vapor. *ACS Nano* **2011**, *5*, 968−974.

(17) Lu, W.; Ruan, G.; Genorio, G.; Zhu, Y.; Novosel, B.; Peng, G.; Tour, J. M. Functionalized Graphene Nanoribbons *via* Anionic Polymerization Initiated by Alkali Metal-Intercalated Carbon Nanotubes. *ACS Nano* **2013**, *7*, 2669−2675.

(18) Sun, Z.; Raji, A.-R. O.; Zhu, Y.; Xiang, C.; Yang, C.; Kittrell, C.; Samuel, E. L.; Tour, J. M. Large-Area Bernal-Stacked Bi-, Tri-, and Tetralayer Graphene. *ACS Nano* **2012**, *6*, 9790−9796.

(19) Malard, L. M.; Pimenta, M. A.; Dresselhaus, G.; Dresselhaus, M. S. Raman Spectroscopy in Graphene. *Phys. Rep.* **2009**, *473*, 51−87.

(20) Park, J. S.; Reina, A.; Saito, R.; Kong, J.; Dresselhaus, G.; Dresselhaus, M. S. G′ Band Raman Spectra of Single, Double and Triple Layer Graphene. *Carbon* **2009**, *47*, 1303−1310.

(21) Cong, C.; Yu, T.; Sato, K.; Shang, J.; Saito, R.; Dresselhaus, G. F.; Dresselhaus, M. S. Raman Characterization of ABA- and ABC-Stacked Trilayer Graphene. *ACS Nano* **2011**, *5*, 8760−8768.

(22) Lui, C. H.; Li, Z.; Chen, Z.; Klimov, P. V.; Brus, L. E.; Heinz, T. F. Imaging Stacking Order in Few-Layer Graphene. *Nano Lett.* **2011**, *11*, 164−169.

(23) Reina, A.; Jia, X.; Ho, J.; Nezich, D.; Son, H.; Bulovic, V.; Dresselhaus, M. S.; Kong, J. Large Area, Few-Layer Graphene Films on Arbitrary Substrates by Chemical Vapor Deposition. *Nano Lett.* **2009**, *9*, 30−35.

(24) Cano-Márquez, A. G.; Rodríguez-Macías, F. J.; Campos-Delgado, J.; Espinosa-González, C. G.; Tristán-López, F.; Ramírez-González, D.; Cullen, D. A.; Smith, D. J.; Terrones, M.; Vega-Cantú, Y. I. Ex-MWNTs: Graphene Sheets and Ribbons Produced by Lithium Intercalation and Exfoliation of Carbon Nanotubes. *Nano Lett.* **2009**, *9*, 1527−1533.

(25) Li, X.; Cai, W.; An, J.; Kim, S.; Nah, J.; Yang, D.; Piner, R.; Velamakanni, A.; Jung, I.; Tutuc, E.; Banerjee, S. K.; Colombo, L.; Ruoff, R. S. Large-Area Synthesis of High-Quality and Uniform Graphene Films on Copper Foils. *Science* **2009**, *324*, 1312−1314.

(26) Ferrari, A. C.; Meyer, J. C.; Scardaci, V.; Casiraghi, C.; Lazzeri, M.; Mauri, F.; Piscanec, S.; Jiang, D.; Novoselov, K. S.; Roth, S.; Geim, A. K. Raman Spectrum of Graphene and Graphene Layers. *Phys. Rev. Lett.* **2006**, *97*, 187401.

(27) Ni, Z.; Wang, Y.; Yu, T.; Shen, Z. Raman Spectra of Misoriented Bilayer Graphene. *Phys. Rev. B* **2008**, *78*, 113407.

(28) Poncharal, P.; Ayari, A.; Michel, T.; Sauvajol, J.-L. Raman Spectroscopy and Imaging of Graphene. *Nano Res.* **2008**, *1*, 273−291.

(29) Cançado, L. G.; Takai, K.; Enoki, T.; Endo, M.; Kim, Y. A.; Mizusaki, H.; Speziali, N. L.; Jorio, A.; Pimenta, M. A. Measuring the Degree of Stacking Order in Graphite by Raman Spectroscopy. *Carbon* **2008**, *46*, 272−275.

(30) Kaniyoor, A.; Ramaprabhu, S. A Raman Spectroscopic Investigation of Graphite Oxide Derived Graphene. *AIP Adv.* **2012**, *2*, 032183.

(31) Ferrari, A. C.; Robertson, J. Interpretation of Raman Spectra of Disordered and Amorphous Carbon. *Phys. Rev. B: Condens. Matter Mater. Phys.* **2000**, *61*, 14095−14107.
(32) Lim, J. K.; Yoo, B. K.; Yi, W.; Hong, S.; Paik, H.; Chun, K.; Kim, S. K.; Joo, S.-W. Photodetachment of Aryl Moieties from Covalently Functionalized Singlewalled Carbon Nanotubes by UV Laser Irradiation. *J. Mater. Chem.* **2006**, *16*, 2374−2379.
(33) Trusovas, R.; Ratautas, K.; Račiukaitis, G.; Barkauskas, J.; Stankevičienė, I.; Niaura, G.; Mažeikienė, R. Reduction of Graphite Oxide to Graphene with Laser Irradiation. *Carbon* **2013**, *52*, 574−582.
(34) Calizo, I.; Ghosh, S.; Bao, W.; Miao, F.; Lau, C. N.; Balandin, A. A. Raman Nanometrology of Graphene: Temperature and Substrate Effects. *Solid State Commun.* **2009**, *149*, 1132−1135.
(35) Graupner, R. Raman Spectroscopy of Covalently Functionalized Single-Wall Carbon Nanotubes. *J. Raman Spectrosc.* **2007**, *38*, 673−683.
(36) Griffiths, J. D. *Introduction to Electrodynamics*, 3rd ed.; Prentice Hall: Englewood Cliffs, NJ, 1999.
(37) Lipson, A.; Lipson, S. G.; Lipson, H. *Optical Physics*; Cambridge University Press: New York, 2011.
(38) De, S.; Lyons, P. E.; Sorel, S.; Doherty, E. M.; King, P. J.; Blau, W. J.; Nirmalraj, P. N.; Boland, J. J.; Scardaci, V.; Joimel, J.; Coleman, J. N. Transparent, Flexible, and Highly Conductive Thin Films Based on Polymer-Nanotube Composites. *ACS Nano* **2009**, *3*, 714−720.
(39) Mirri, F.; Ma, A. W. K.; Hsu, T.; Behabtu, N.; Eichmann, S. L.; Young, C. C.; Tsentalovich, D. E.; Pasquali, M. High-Performance Carbon Nanotube Transparent Conductive Films by Scalable Dip Coating. *ACS Nano* **2012**, *6*, 9737−9744.
(40) De, S.; Higgins, T. M.; Lyons, P. E.; Sorel, S.; Doherty, E. M.; King, P. J.; J. Blau, W. J.; Nirmalraj, P. N.; Blau, W. J.; Boland, J. J.; Coleman, J. N. Silver Nanowire Networks as Flexible, Transparent, Conducting Films: Extremely High DC to Optical Conductivity Ratios. *ACS Nano* **2009**, *3*, 1767−1774.
(41) De, S.; King, P. J.; Lotya, M.; O'Neill, A.; Doherty, E. M.; Hernandez, Y.; Duesberg, G. S.; Coleman, J. N. Flexible, Transparent, Conducting Films of Randomly Stacked Graphene from Surfactant-Stabilized, Oxide-Free Graphene Dispersions. *Small* **2010**, *6*, 458−464.
(42) Zhu, Y.; Lu, W.; Sun, Z.; Kosynkin, D. V.; Yao, J.; Tour, J. M. High Throughput Preparation of Large Area Transparent Electrodes Using Non-Functionalized Graphene Nanoribbons. *Chem. Mater.* **2011**, *23*, 935−939.